Eurasian contribution to the last glacial dust cycle: how are loess sequences built?

Denis-Didier Rousseau[1,2], Anders Svensson[3], Matthias Bigler[4], Adriana Sima[1], Jorgen Peder Steffensen[3] and Niklas Boers[1].

[1]Ecole Normale Supérieure, UMR CNRS 8539, Laboratoire de Météorologie Dynamique, and CERES-ERTI, 24 rue Lhomond, 75231 Paris cedex 5, France

[2]Lamont-Doherty Earth Observatory of Columbia University, Palisades, NY 10964, USA

[3]Centre for Ice and Climate Niels Bohr Institute, University of Copenhagen, Juliane Maries Vej 30, DK-2100 Copenhagen OE, Denmark

[4]University of Bern, Physics Institute, Climate and Environment Physics, Sidlerstrasse 5, CH-3012 Bern, Switzerland

Correspondence to: Denis-Didier Rousseau (denis.rousseau@lmd.ens.fr)

Key words: Palaeoclimatology, Glaciology, Geomorphology, Atmospheric science, Climate Science, Geophysics, Oceanography, loess

Abstract. The last 130,000 years have been marked by pronounced millennial scale climate variability, which strongly impacted the terrestrial environments of the Northern Hemisphere especially at middle latitudes. Identifying the trigger of these variations, which are most likely associated with strong couplings between the ocean and the atmosphere, still remains a key question. Here, we show that the analysis of $\delta^{18}O$ and dust in the Greenland ice cores, and a critical study of their source variations, reconciles these records with those observed on the Eurasian continent. We demonstrate the link between European and Chinese loess sequences, dust records in Greenland, and variations of the North Atlantic sea ice extent. The sources of the emitted and transported dust material are variable and relate to different environments corresponding to present desert areas, but also hidden regions related to lower sea level stands, dry rivers, or zones close to the frontal moraines of the main Northern Hemisphere ice sheets. We anticipate our study to be at the origin of more sophisticated and elaborated investigations of millennial and sub-millennial continental climate variability on the Northern Hemisphere.

1 Introduction

During the last glacial interval, abrupt climate changes have been documented worldwide in different types of records, but especially in ice cores (Dansgaard et al., 1969, 1982; Johnsen et al., 1992; Johnsen et al., 1972, 2001). Their interpretation mostly focused on the more spectacular character corresponding to abrupt warmings (named Dansgaard-Oeschger -DO- events, Broecker et al., 1990) of some ten degrees to interstadial conditions in Greenland (Kindler et al., 2014). These warmings were followed by a schematic two-step return to stadial conditions. Modeling experiments are able to reconstruct this abrupt warming and the two-step return to stadial conditions, indicating a periodicity of about 1500 years (Schulz, 2002; Rahmstorf, 2003) which, however, still remains questionable (Ditlevsen et al., 2007; Thomas et al., 2011; Boers et al., 2017). More precisely, the very high-resolution analysis of the last deglaciation in the North Greenland Ice Core Project (NGRIP) record (North Greenland Ice Core Project, 2004), Greenland, revealed that different parameters show different abruptness of the warming events. For the last two warming events (14.7 and 11.7 ka b2k), deuterium excess increased within one to three years, alongside with more gradually increasing temperatures as represented by $\delta^{18}O$. Dust concentration would require at least fifteen years to decrease, preceding the deuterium excess increase by 10 ± 5 years (Steffensen et al., 2008). Considering carefully the DO events noticed during the last climatic cycle in NGRIP, some variability that occurs as the last deglaciation timing of transitions does not seem to reproduce every time in the older parts of the record (Rousseau et al., 2017). The climate trend, cooling and increase in dustiness, within these particular events is variable as well. High-resolution studies of the temperature signal in older interstadials show the occurrence of sub-millennial scale elements like precursor events of about centennial duration before the interstadial itself, rebound events exhibiting abrupt cooling towards stadial conditions, and cooling events occurring towards the end of the interstadial (Capron et al., 2010). These sub-millennial events make the understanding of the climate variability during these interstadials even more complicated than a simple warming followed by a two-step cooling. Ice cores nevertheless provide much more information than on temperature and dust concentration only, as they release records of numerous components of the climate system, isotope values of the transported water vapor, mineral aerosols and greenhouse gas concentrations, chemical elements, etc., which show different origins and transport patterns to the high latitude ice-sheets. Such richness in proxies allows comparisons with other records of millennial scale variability preserved in both marine (Henry et al., 2016) and terrestrial deposits, as well as in other ice cores (Barbante et al., 2006; Buizert et al., 2015). In this paper, after briefly describing the abrupt changes observed in the very high resolution $\delta^{18}O$ and dust records from NGRIP (North Greenland Ice Core Project, 2004), we compare the dust particle sedimentation rates over Europe and China as expressed in key loess sequences (Fig. 1). This is a complementary study of Rousseau et al. (2017), which essentially focused on paleosol development. In the last section we provide an interpretation of the link between Greenland dust records and Eurasian loess sequence development.

2 Analysis

We investigate in this study the 18 Greenland interstadials (GI), labeled from 17.1 to 2 (Rasmussen et al., 2014), which have been identified during the MIS 3 and 2 (59 – 14 ka b2k) interval. We performed this comparison by studying in parallel the $\delta^{18}O$ (NGRIP members, 2004; Gkinis et al., 2014) and the dust (Ruth et al., 2003) records from the NGRIP ice core at the highest resolution. These two indices correspond to different sources, marine and continental, respectively, but also to different origins, mostly Atlantic (Masson-Delmotte et al., 2006) and East Asian (Biscaye et al.,

1997; Svensson et al., 2000; Bory et al., 2002), respectively. The two indices are not directly related so that if similarities would appear, this should highlight a more global phenomenon.

The compilation of the 18 GI in the NGRIP record (Rousseau et al., 2017) shows that DO events can be characterized using a numerical algorithm (see supplementary material) by an increase of $\delta^{18}O$ occurring on average in 36.4 ± 13.4 (1σ) years, with a mean GI duration of 1048 ± 1163 (1σ) years (Tab. 1). When determined visually by considering the onset of the abrupt change at the start and the return to the same initial value as the end of the event, the $\delta^{18}O$ changes occur, on average, in 55.4 ± 16.1 (1σ) years, with a mean duration of 1053 ± 1068 (1σ) years. The larger errors than the mean values are due to the few long intervals. These two methods have been described in detail in Rousseau et al. (2017). Although both methods allow identifying the GI and their parameters (onset, transition and duration), the numerical approach allows also to identify statistically significant events that the virtual one could consider as questionable. However, we consider that these two methods are complementary, the reason why we decided to release values obtained by both of them. These compiled characteristics fit with the values generally considered from the literature (Wolff et al., 2010; Rasmussen et al., 2014;).

Following the detailed correlations defined between Nussloch and NGRIP stratigraphies (Fig. 2) (Rousseau et al., 2002, 2007b, 2017), we then applied the dates obtained for every start and end of a GI, from both the $\delta^{18}O$ and the dust NGRIP timescale, to the loess sequence. This was performed by considering that in west European loess sequences, paleosols developed from the underlying loess deposits after a stop of the eolian sedimentation (Taylor et al., 2014), and that the eolian sedimentation itself restarted on top of the developed paleosols. This makes the time evolution non-linear and a bit more complex, than the classical continuous sedimentation observed in other terrestrial, marine, and ice core records (Kukla and Koci, 1972; Rousseau et al., 2007a). Therefore, a determined eolian interval, equivalent to a Greenland stadial (GS), includes the loess unit and the overlying paleosol (blue arrow in Figure 3), while the paleosol development itself fits with the GI duration (red arrow in Figure 3). Doing so, the Nussloch stratigraphy can be read as expressed in Table 2, allowing then to better estimate the sedimentation and the mass accumulation rates required for comparison with other loess records and model outputs. In Chinese loess sequences on the contrary, no such paleosols developed during the last climate cycle. Therefore, own reasoning do not apply to these records.

3 Discussion

Mineral dust record in the NGRIP ice core is obtained from variations in dust concentration, measured in the terms of the number of particles larger than 1 micron per milliliter of melt water, which shows also abrupt changes that are quite synchronous to the DO events expressed in the $\delta^{18}O$ record (Mayewski et al., 1994; Ruth et al., 2003; North Greenland Ice Core Project, 2004; Rasmussen et al., 2014). Abrupt decreases in the dust concentration occur in 60 ± 21.2 (1σ) years on average, with a mean GI duration of 1079 ± 1135 (1σ) years when determined with the same algorithm as for $\delta^{18}O$; when determined visually, the dust decrease occurs in 56.8 ± 19.6 (1σ) years on average, with a mean duration of 1079 ± 1079 (1 s) years (Tab. 1). Interestingly, the dust change reaches its minimum value on average about 6 years after the $\delta^{18}O$. These abrupt changes also correspond to abrupt temperature differences of on average 11.6 ± 2.7 (1σ) °C for the GI 17.1 to 2 (Kindler et al., 2014) Tab. 1). The amplitude of the change in the dust concentration corresponds in average to a factor of 6 in about 57 years. These values are different from previous investigations of the GRIP dust

record, which were showing much more rapid changes in a few years, but they seem more realistic than extremely abrupt shifts that would be particularly difficult to interpret from a dynamical point of view.

Isotope studies of the dust recorded in the Greenland ice cores demonstrated an Asian origin for both summer and winter seasons (Biscaye et al., 1997; Svensson et al., 2000), while the analysis of modern dust preserved in modern firn indicates a different origin for summer (essentially Takla Makan) and winter (Takla Makan and northern Chinese and Mongolian deserts) (Bory et al., 2002). The transport of the modern chemical aerosols towards Greenland also partly supports an Asian origin and therefore allows interpreting the dust record in the ice cores (Goto-Azuma and Koerner, 2001). Indeed, the major dust event recorded in China in April 6, 2001, the largest ever-recorded dust storm worldwide, provides relevant information about the Asian dust transport, past and present, towards Northern Hemisphere ice-sheets. The identification of the dust particles related to this event on top of Mt Logan, Alaska, indicates that the assumption of Asian dust origin also in the past is particularly adequate (Zdanowicz et al., 2006). The presence of the large Laurentide ice-sheet over North America at least at the last glacial maximum caused a split of the polar jet stream, inducing two main pathways for the Asian fine dust transport eastwards (Fig. 4). A comparison of the different GI dust records indicates that the dust concentration falls in about 60 years by a factor of 8 from the beginning of the warming during DO events. These values are similar to the variations of a factor of 5 to 7 during four decades observed during the 15.5 - 11.5 ka b2k interval (Steffensen et al., 2008). Reducing so drastically the dust concentration in the ice core implies a similar drastic reduction of the dust concentration in the atmosphere, relying on changes in the sources, in the transport, and/or in the deposition of the particles (Fischer et al., 2007).

Concerning the changes in the sources, several points can be taken into consideration. At present the amount of dust emitted from different Chinese deserts into the atmosphere occurs mostly in April, about 43.4% of the 1,451 Mt of dust emitted from 1996 to 2001 (Laurent et al., 2006). However, these sources do not behave similarly. While the average quantity of dust annually emitted is similar in the Gobi and Takla Makan deserts, the frequency of the dust storms are different, more numerous in the Takla Makan than in the Gobi (Laurent et al., 2005). A reduction in the size of these sources does not seem to be a reliable cause, as these deserts did not vary much in the relevant past (Rittner et al., 2016). Therefore, a reduction in the availability of dust material should be sought by considering atmospheric circulation changes. Studying the ESR intensity signal from marine core MD01-2407 from the Japan Sea, Nagashima et al. (2011) have shown that Mongolian Gobi source was dominant during GS while Takalamakan soirce was dominant source during GI, with some variation between the interstadials. The analysis of Chinese speleothems from caves located southward of the Chinese Loess Plateau (CLP) indicates millennial-scale variations in the stalagmite growth, related to variations in precipitation over the cave area linked to stronger summer monsoon activity, which are synchronous to the GI (Wang et al.., 2001, 2008). From two key Chinese loess sequences, Sun et al. (2012) have described abrupt millennial-scale changes expressed by detailed synchronous mean grain size variations over the 60-10 ka b2k interval in deposited wind blown material, from coarser material during GS to thinner particles during GI. The sedimentation rate estimated from the key sequences of Jingyuan and Gulang varies between 6 and 63 cm/kyr for Jingyuan and between 10 and 130 cm/kyr for Gulang, respectively (Fig. 4). Therefore, as meridional circulation prevailed at least in Eastern Asia due to the monsoonal system, aridity could have been reduced during the favorable season (around April, with some variation, delay, depending of GS or HS as observed in eastern Europe by Sima et al., (2013)) of dust emission of these short intervals (Sun et al., 2012). A recent study of the decline of the snow cover over Northeast Russia, Southwest Asia and Northern India, Tibetan Plateau, reports the snow cover decline creates favorable

dynamical conditions for strong winds over the Arabian Sea and thus favoring a stronger summer monsoon (Goes et al., 2005). Complementarily, a modeling experiment indicates that a strong East Asian monsoon could be related to planetary waves related to the extension of the Northern Hemisphere ice sheets, affecting the precipitation band at the latitude of the CLP (Yin et al., 2008). However, as the main interval for dust emission is April, one can hardly assume the summer monsoon as the main driver of a reduction of dust emissions. On the contrary, modern East Asian dust storms are related to surges of cold air originating from Siberia, and such conditions should have been reduced during the GI compared to GS at least during April, the main dust emission season. Reduced cold outbreaks could have resulted from the reduction of the snow cover due to warming Eurasia and to a negative feedback related to dust deposition on snow as deduced from another modeling experiment (Krinner et al., 2006).

Europe has been strongly impacted by these North Atlantic millennial-scale climate changes, as observed in different types of deposits (Genty et al., 2003; Müller et al., 2003; Rousseau et al., 2002, 2007b) (Fig. 1). The influence of the westerlies and the position of the polar jet stream were constrained by the variation in the extension of the sea ice during the last glacial interval (Sima et al. , 2009; 2013). Furthermore, the presence of ice sheets over Great Britain, Scandinavia and of an ice cap over the Alps enhanced the zonal circulation that reflects the location of the thickest loess deposits (Fig. 1B). Extensive investigation of European loess series along a west to east transect at 50°N (Fig. 1B) reveals that the millennial-scale climate variations observed in the North Atlantic are preserved in these particular eolian deposits (2009; Antoine et al., 2001; Rousseau et al., 2002; 2007b). They clearly show alternating loess and paleosol units, which are continental equivalents, respectively, to the GS and GI (Moine et al., 2017; Rousseau et al., 2017) (Fig. 2, 3). The Nussloch loess sequence along the Rhine valley is the most detailed record for the interval 50 to 15 ka b2k. The nature of the observed paleosols is related to the duration of the corresponding GI themselves (Rousseau et al., 2017): GI8, the longest of the last 8 GI, is represented in Nussloch by a brown arctic soil, while the youngest GI correspond to tundra gleys or embryonic soils (oxidized horizons) for GI3 and GI2, which are particularly short (Antoine et al., 2009; Rousseau et al., 2002; 2007b) (Fig. 2, 3). An estimate of the duration of the continental equivalent of GI can be deduced from the Greenland dust record by considering the interval after the abrupt warming, when the dust concentration was minimum in the atmosphere and therefore shows low values in the Greenland ice cores. Such succession is observed over a more than 2000 km wide area from Western Europe eastward to Ukraine during the last climatic cycle (Rousseau et al., 2011), showing the influence of the zonal circulation, as it is the case in modern time (Fig. 5 A, B). In the Nussloch key sequence, the sedimentation rate of dust particles varies between 23 and 157 cm/kyr for the loess units synchronous to GS. These values are similar to those observed in the Northern edge of the CLP by Sun et al. (2012) (Tab. 2, Fig. 1A, 4), supporting an apparently similar eolian characteristic within a more global dynamics. Furthermore, modeling experiments show that dust emission mainly occurred in April (Sima et al., 2009) as nowadays in modern deserts, although the European sources are not deserts at all presently. These modeling studies also indicate that the zonal circulation not only prevailed during the GI intervals, but also during the GS as recorded by loess deposits. For the coarsest material these eolian units are composed of material of local and regional (up to about 500 km) origin, mainly from dried river beds (Rousseau et al., 2014). The finest grains originate from longer distances, but still from deflation areas, mostly located in the emerged English Channel, North Sea or Northern European plain, and at the margin of the Fennoscandian frontal moraines (Sima et al., 2009; Rousseau et al., 2014) (Fig. 1B). Since in Kurtak, Siberia (Fig. 1A, 4) we observe similar and synchronous alternations between eolian loess units and paleosols to those observed over Europe (Haesaerts et al., 2005), we infer that a zonal circulation similar to the present one (Fig. 5) was prevailing over Eurasia during both GS and GI, synchronizing the loess-paleosol sequences between Europe and Asia

(Haesaerts et al., 2005). The initial warming over Greenland and the North Atlantic is transported eastward by the prevailing zonal circulation. As explained above, this propagating warming should have reduced the production of cold surges contributing to the strong atmospheric dynamics (Sun et al., 2012) responsible for the dust emission in Northern Chinese deserts, which are the main dust suppliers of both CLP and Greenland ice-sheet. The stronger winds during GS and weaker winds during GI permitted the record of DO-like intervals in Chinese loess sequences through grain size variations with coarser material deposition during GS and finer during GI (Sun et al., 2012).

All the mechanisms described above involve the Northern Hemisphere and do not address the origin of these abrupt changes. Recent investigations in Antarctic ice core WAIS (Buizert et al., 2015) have demonstrated the north-to-south directed transfer of the abrupt changes with Greenland warmings leading Antarctic coolings; the associated heat transfer is argued to be modulated by the Atlantic Meridional Overturning Circulation rather than by the atmosphere (Henry et al., 2016). Although the origin of the DO events is not yet elucidated, the Northern Atlantic changes still remain the drivers of those observed over Eurasia. Indeed, the modern cyclonic pattern of moisture transport towards the Greenland ice sheet (Masson-Delmotte et al., 2006) depends on the sea surface conditions over the North Atlantic Ocean and clear pathways of this transport have been identified (Chen et al., 1997). During the last climate cycle, this pattern was related to both the sea ice extent and the size and expansion of the Laurentide ice sheet in North America, which impacts the Northern Hemisphere atmospheric circulation (Kutzbach, 1987). The large changes in deuterium excess at the onset of the warming reveal large variations in the moisture source regions. These variations are most likely associated with changes in sea-ice extent, which shift the source regions, combined with changes in atmospheric circulation patterns (Masson-Delmotte et al., 2006 Sodermann et al. 2008, 2010).). Due to the changing albedo, sea-ice extent itself directly impacts the atmospheric circulation. On the other hand, sea ice is mainly driven by the meridional overturning oscillation, which would have thus induced the observed $\delta^{18}O$ and hence temperature changes noticed on the Greenland ice cores (Henry et al., 2016). In turn, this would have also impacted the Northern Hemisphere atmospheric circulation, contributing to the abrupt millennial-scale changes including the DO events in Eurasian terrestrial records. At middle latitude these changes constrained the emission of local and regional dust particles, their transport and their deposition in the loess sequences, which can be characterized by similar sedimentation rates over the area corresponding to a general climate dynamics, but nevertheless different mass accumulation rates (MAR) related to the bedrock of the source areas of the deposited material. In a previous study, Kohfeld and Harrison (2003) estimated MAR over CLP varying between 21 and 809 $g/m^2/yr$ for MIS 3 and between 60 and 5238 $g/m^2/yr$ for MIS 2. In Europe, Frechen et al. (2003), applying the same method, indicate MAR varying between 100 and 7000 $g/m^2/yr$ with particular high values for Nussloch (1213-6129 $g/m^2/yr$). These estimates are higher than those determined in our study after re-evaluation of the chronology of the key sequence, still following the same calculation, which yields MAR varying values between 376 and 2586 $g/m^2/yr$ (376 – 1952 $g/m^2/yr$ for MIS3 and 724 - 2586 $g/m^2/yr$ for MIS2) or between 395 and 2515 $g/m^2/yr$ (395 - 1952 $g/m^2/yr$ for MIS3 and 723 - 2515 $g/m^2/yr$ for MIS2) when considering the $\delta^{18}O$ and dust related NGRIP chronologies, respectively (Tab. 2). Still, as Nussloch represent an exceptional record of MIS 3 and 2, we consider our results as corresponding to the highest boundary values for this time interval in European deposits.

4 Conclusion

Our study thus shows that a strong emphasis has to be placed on the past dust record, which is still poorly understood and weakly integrated in general circulation models. The important uncertainties associated with mineral aerosols in the recent IPCC report (Solomon et al., 2007) are a clear indication that more must be done on this particular parameter.

Because this is a key factor in the climate system, understanding the past dust cycle is an important requirement, especially when estimating the dust load in the past atmospheres, and this should open new fields of investigation for a better constraint of the climate variability in different contexts.

The present study provides new insights in the analysis of the millennial scale variability and of abrupt climate changes by proposing the links gathering atmospheric, marine and continental records. It shows that the complete understanding of the whole climate system requires investigations at high resolution in every domain with the support of modeling experiments. In the present study, we show that both $\delta^{18}O$ increase and dust decrease take place over an interval of about 50 years on average from the start of the abrupt change. This corresponds to the four decades previously mentioned for the two warmings occurring during the 15.5-11.5 ka b2k interval, which are associated with strong resumptions of the meridional overturning circulation (McManus et al., 2004). This makes the potential change in the atmospheric dynamics more reliable. Our investigation provided an explanation of the record of the abrupt climate changes in the northern hemisphere dust records, both in the Greenland ice sheet and over Eurasia. It shows that dust should be considered one of the major players of the past climate millennial variability.

Acknowledgments

DDR and AS are partly supported by ANR Research grant (ACTES: ANR08-BLAN-0227 - CSD 6). AS, MB and JPS are supported by NGRIP. NGRIP is directed and organized by the Ice and Climate research group, Niels Bohr Institute, University of Copenhagen. It is supported by funding agencies in Denmark (FNU), Belgium (FNRS-CFB), France (IPEV and INSU/CNRS), Germany (AWI), Iceland. (RannIs), Japan (MEXT), Sweden (SPRS), Switzerland (SNF) and the USA (NSF, Office of Polar Programs). NB acknowledges funding by the Alexander von Humboldt Foundation and the German Federal Ministry for Education and Research. This work started thanks to the support of our dear colleague and friend Dr. Sigfus Johnsen to who it is dedicated. Eric Wolff and Jerry McManus are thanked for providing useful comments on drafts of that paper which strongly improved it. CNRS-INSU rejected a support request to DDR for the completion of this study because of the lack of innovation and interest but hopefully thoughts remain free.

The used data sets in this study are available at " www.icecores.dk"

Authors contributions

DD Rousseau designed research, DDR, SJJ, AS, MB, AS and JPS performed research, SJJ, AS, MB and JPS performed drilling and analysis of NGRIP ice core, AS performed modeling experiment, DDR designed and performed loess sequences investigation, DDR performed the new Nussloch chronological sequence, calculated the associated sedimentation rates and MARs, NB performed the algorithmic determination of the DO events in both $\delta^{18}O$ and dust NGRIP records, DDR, NB and AS wrote the paper.

References

Antoine, P., Coutard, S., Guerin, G., Deschodt, L., Goval, E., Locht, J.L., Paris, C. (2016). Upper Pleistocene loess-palaeosol records from Northern France in the European context: Environmental background and dating of the Middle Palaeolithic. Quaternary international 411, 4-24, doi: 10.1016/j.quaint.2015.11.036, 2016

Antoine, P., Rousseau, D.D., Moine, O., Kunesch, S., Hatte, C., Lang, A., Tissoux, H., and Zöller, L.: Rapid and cyclic aeolian deposition during the Last Glacial in European loess: a high-resolution record from Nussloch, Germany. Quaternary Sci. Rev. 28, 2955-2973, doi: 10.1016/j.quascirev.2009.08.001, 2009.

Antoine, P., Rousseau, D.D., Zöller, L., Lang, A., Munaut, A.V., Hatté, C., and Fontugne, M.: High-resolution record of the last interglacial-glacial cycle in the loess palaeosol sequences of Nussloch (Rhine Valley-Germany). Quatern. Int. 76/77, 211-229, doi: 10.1016/S1040-6182(00)00104-X, 2001.

Barbante, C., Barnola, J.M., Becagli, S., Beer, J., Bigler, M., Boutron, C., Blunier, T., Castellano, E., Cattani, O., Chappellaz, J., Dahl-Jensen, D., Debret, M., Delmonte, B., Dick, D., Falourd, S., Faria, S., Federer, U., Fischer, H., Freitag, J., Frenzel, A., Fritzsche, D., Fundel, F., Gabrielli, P., Gaspari, V., Gersonde, R., Graf, W., Grigoriev, D., Hamann, I., Hansson, M., Hoffmann, G., Hutterli, M.A., Huybrechts, P., Isaksson, E., Johnsen, S., Jouzel, J., Kaczmarska, M., Karlin, T., Kaufmann, P., Kipfstuhl, S., Kohno, M., Lambert, F., Lambrecht, A., Lambrecht, A., Landais, A., Lawer, G., Leuenberger, M., Littot, G., Loulergue, L., Luthi, D., Maggi, V., Marino, F., Masson-Delmotte, V., Meyer, H., Miller, H., Mulvaney, R., Narcisi, B., Oerlemans, J., Oerter, H., Parrenin, F., Petit, J.R., Raisbeck, G., Raynaud, D., Rothlisberger, R., Ruth, U., Rybak, O., Severi, M., Schmitt, J., Schwander, J., Siegenthaler, U., Siggaard-Andersen, M.L., Spahni, R., Steffensen, J.P., Stenni, B., Stocker, T.F., Tison, J.L., Traversi, R., Udisti, R., Valero-Delgado, F., van den Broeke, M.R., van de Wal, R.S.W., Wagenbach, D., Wegner, A., Weiler, K., Wilhelms, F., Winther, J.G., Wolff, E., and Members, E.C.: One-to-one coupling of glacial climate variability in Greenland and Antarctica. Nature 444, 195-198, doi: 10.1038/nature05301, 2006.

Biscaye, P.E., Grousset, F.E., Revel, M., Van der Gaast, S., Zielinski, G.A., Vaars, A., and Kukla, G., Asian provenance of glacial dust (Stage 2) in the GISP2 ice core, summit, Greenland. J. Geophys. Res. 102, 26,765-26,781, doi:10.1029/97JC01249, 1997.

Boers, N., Chekroun, M.D., Liu, H., Kondrashov, D., Rousseau, D.-D., Svensson, A., Bigler, M., Ghil, M.: Inverse stochastic-dynamic models for high-resolution Greenland ice-core records. Earth Syst. Dynam Discussion, doi: 10.5194/esd-2017-8, 2017.

Bory, A.J.M., Biscaye, P.E., Svensson, A., and Grousset, F.E.: Seasonal variability in the origin of recent atmospheric mineral dust at NorthGRIP, Greenland. Earth Planet. Sc. Lett.196, 123-134, doi: 10.1016/S0012-821X(01)00609-4, 2002.

Broecker, W., Bond, G., and Klas, M.: A salt oscillator in the glacial Atlantic? 1. The concept. Paleoceanography 5, 469-477, doi: 10.1029/PA005i004p00469, 1990.

Buizert, C., Adrian, B., Ahn, J., Albert, M., Alley, R.B., Baggenstos, D., Bauska, T.K., Bay, R.C., Bencivengo, B.B., Bentley, C.R., Brook, E.J., Chellman, N.J., Clow, G.D., Cole-Dai, J., Conway, H., Cravens, E., Cuffey, K.M., Dunbar, N.W., Edwards, J.S., Fegyveresi, J.M., Ferris, D.G., Fitzpatrick, J.J., Fudge, T.J., Gibson, C.J., Gkinis, V., Goetz, J.J., Gregory, S., Hargreaves, G.M., Iverson, N., Johnson, J.A., Jones, T.R., Kalk, M.L., Kippenhan, M.J., Koffman, B.G., Kreutz, K., Kuhl, T.W., Lebar, D.A., Lee, J.E., Marcott, S.A., Markle, B.R., Maselli, O.J., McConnell, J.R., McGwire, K.C., Mitchell, L.E., Mortensen, N.B., Neff, P.D., Nishiizumi, K., Nunn, R.M., Orsi, A.J., Pasteris, D.R., Pedro, J.B., Pettit, E.C., Price, P.B., Priscu, J.C., Rhodes, R.H., Rosen, J.L., Schauer, A.J., Schoenemann, S.W., Sendelbach, P.J., Severinghaus, J.P., Shturmakov, A.J., Sigl, M., Slawny, K.R., Souney, J.M., Sowers, T.A., Spencer, M.K., Steig, E.J., Taylor, K.C., Twickler, M.S., Vaughn, B.H., Voigt, D.E., Waddington, E.D., Welten, K.C., Wendricks, A.W., White, J.W.C., Winstrup, M., Wong, G.J., Woodruff,

T.E., and Members, W.D.P.: Precise interpolar phasing of abrupt climate change during the last ice age. Nature 520, 661-U169, doi: 10.1038/nature14401, 2015.

Capron, E., Landais, A., Chappellaz, J., Schilt, A., Buiron, D., Dahl-Jensen, D., Johnsen, S.J., Jouzel, J., Lemieux-Dudon, B., Loulergue, L., Leuenberger, M., Masson-Delmotte, V., Meyer, H., Oerter, H., Stenni, B.: Millennial and sub-millennial scale climatic variations recorded in polar ice cores over the last glacial period. Clim. Past 6, 345-365, doi: 10.5194/cp-6-345-2010, 2010.

Chen, Q.S., Bromwich, D.H., and Bai, L.S.: Precipitation over Greenland retrieved by a dynamic method and its relation to cyclonic activity. J. Climate 10, 839-870, doi: 10.1175/1520-0442(1997)010<0839:POGRBA>2.0.CO;2, 1997.

Dansgaard, W., Clausen, H.B., Gundestrup, N., Hammer, C.U., Johnsen, S.F., Kristinsdottir, P.M., and Reeh, N.: A new Greenland deep ice core. Science 218, 1273-1277, doi: 10.1126/science.218.4579.1273, 1982.

Dansgaard, W., Johnsen, S.J., Moller, J., and Langway, C.C.: One thousand centuries of climatic record from Camp Century on the Greenland ice sheet. Science 166, 377-381, doi: 10.1126/science.166.3903.377, 1969.

Ditlevsen, P.D., Andersen, K.K., Svensson, A.: The DO-climate events are probably noise induced: statistical investigation of the claimed 1470 years cycle. Clim. Past 3, 129-134, 2007.

Fischer, H., Siggaard-Andersen, M.-L., Ruth, U., Rothlisberger, R., and Wolff, E.: Glacial/interglacial changes in mineral dust and sea-salt records in polar ice cores: Sources, transport, and deposition. Rev. Geophys. 45, doi: 10.1029/2005RG000192, 2007.

Frechen, M., Oches, E.A., and Kohfeld, K.E.: Loess in Europe-mass accumulation rates during the Last Glacial Period. Quaternary Sci. Rev. 22, 1835-1857, doi: 10.1016/S0277-3791(03)00183-5, 2003.

Genty, D., Blamart, D., Ouahdi, R., Gilmour, M., Baker, A., Jouzel, J., and Van-Exter, S.: Precise dating of Dansgaard-Oeschger climate oscillations in western Europe from stalagmite data. Nature 421, 833-837, doi: 10.1038/nature01391, 2003.

Gkinis, V., Simonsen, S. B., Buchardt, S. L., White, J. W. C., Vinther, B. M.: Water isotope diffusion rates from the NorthGRIP ice core for the last 16,000 years – Glaciological and paleoclimatic implications. Earth and Planetary Science Letters, 405, 132-141. DOI: 10.1016/j.epsl.2014.08.022, 2014.

Goes, J.I., Thoppil, P.G., Gomes, H.D., and Fasullo, J.T.: Warming of the Eurasian landmass is making the Arabian Sea more productive. Science 308, 545-547, doi: 10.1126/science.1106610, 2005.

Goto-Azuma, K., and Koerner, R.M.: Ice core studies of anthropogenic sulfate and nitrate trends in the Arctic. J. Geophys. Res. 106, 4959-4969, doi: 10.1029/2000JD900635, 2001.

Haesaerts, P., Chekha, V.P., Damblon, F., Drozdov, N.I., Orlova, L.A., and Van der Plicht, J.: The loess-palaeosol succession of Kurtak (Yenisei Basin, Siberia): a reference record for the Karga stage (MIS 3). Quaternaire 16, 3-24, 2005.

Henry, L.G., McManus, J.F., Curry, W.B., Roberts, N.L., Piotrowski, A.M., and Keigwin, L.D.: North Atlantic ocean circulation and abrupt climate change during the last glaciation. Science 353, 470-474, doi: 10.1126/science.aaf5529, 2016.

Hodell, D.A., Evans, H.F., Channell, J.E.T., and Curtis, J.H. Phase relationships of North Atlantic ice-rafted debris and surface-deep climate proxies during the last glacial period. Quaternary Sci. Rev. 29, 3875-3886, doi: 10.1016/j.quascirev.2010.09.006 , 2010.

Johnsen, S.J., Clausen, H.B., Dansgaard, W., Fuhrer, K., Gundestrump, N., Hammer, C.U., Iversen, P., Jouzel, J., Stauffer, B., and Steffensen, J.P.: Irregular glacial interstadials recorded in a new Greenland ice core. Nature 359, 311-313, doi: 10.1038/359311a0,1992.

Johnsen, S.J., Dahl-Jensen, D., Gundestrup, N., Steffensen, J.P., Clausen, H.B., Miller, H., Masson-Delmotte, V., Sveinbjörnsdottir, A.E., and White, J.: Oxygen isotope and palaeotemperature records from six Greenland ice-core stations: Camp Century, Dye-3, GRIP, GISP2, Renland and NorthGRIP. J. Quaternary. Sci. 16, 299-307, doi: 10.1002/jqs.622 , 2001.

Johnsen, S.J., Dansgaard, W., Clausen, H.B., and Langway, C.C.: Oxygen isotope profiles through the Antartic and Greenland ice sheets. Nature 235, 429-434, doi: 10.1038/235429a0, 1972.

Kindler, P., Guillevic, M., Baumgartner, M., Schwander, J., Landais, A., and Leuenberger, M. NGRIP temperature reconstruction from 10 to 120 kyr b2K. Clim. Past 9, 4099-4143, doi: 10.5194/cp-10-887-2014, 2014.

Kohfeld, K.E., and Harrison, S.P. Glacial-interglacial changes in dust deposition on the Chinese Loess Plateau. Quaternary Sci. Rev. 22, 1859-1878, doi: 10.1016/S0277-3791(03)00166-5, 2003.

Krinner, G., Boucher, O., and Balkanski, Y.: Ice-free glacial northern Asia due to dust deposition on snow. Clim. Dyn. 27, 613-625, doi: 10.1007/s00382-006-0159-z, 2006.

Kukla, G.J., and Koci, A.: End of the last interglacial in the loess record. Quaternary. Res. 2, 374-383, 1972.

Kutzbach, J.E.: Model simulations of the climatic patterns during the deglaciation of North America, in: Ruddiman, W.F., Wright, H.E. (Eds.), North America and Adjacent Oceans during the Last Deglaciation - The Geology of North America. The Geological Society of America, Boulder, pp. 425-446, 1987.

Laurent, B., Marticorena, B., Bergametti, G., Chazette, P., Maignan, F., and Schmechtig, C.: Simulation of the mineral dust emission frequencies from desert areas of China and Mongolia using an aerodynamic roughness length map derived from the POLDER/ADEOS 1 surface products. J. Geophys. Res.-Atmospheres 110. D18S04, doi: 10.1029/2004JD005013, 2005.

Laurent, B., Marticorena, B., Bergametti, G., and Mei, F.: Modeling mineral dust emissions from Chinese and Mongolian deserts. Global Planet. Change 52, 121-141, doi: 10.1016/j.gloplacha.2006.02.012, 2006.

Masson-Delmotte, V., Dreyfus, G., Braconnot, P., Johnsen, S., Jouzel, J., Kageyama, M., Landais, A., Loutre, M.F., Nouet, J., Parrenin, F., Raynaud, D., Stenni, B., and Tuenter, E.: Past temperature reconstructions from deep ice cores: relevance for future climate change. Clim. Past 2, 145-165, 2006.

Mayewski, P.A., Meeker, L.D., Whitlow, S., Twickler, M.S., Morrison, M.C., Bloomfield, P., Bond, G.C., Alley, R.B., Gow, A.J., Grootes, P.M., Meese, D.A., Ram, M., Taylor, K.C., and Wumkes, W.: Changes in atmospheric circulation and ocean ice cover over the North Atlantic during the last 41,000 years. Science 263, 1747-1751, doi: 10.1126/science.263.5154.1747, 1994.

McManus, J.F., Francois, R., Gherardi, J.M., Keigwin, L.D., and Brown-Leger, S.: Collapse and rapid resumption of Atlantic meridional circulation linked to deglacial climate changes. Nature 428, 834-837, doi: 10.1038/nature02494, 2004.

Moine, O., Antoine, P., Hatté, C., Landais, A., Mathieu, J., Prud'Homme, C., and Rousseau, D.-D.: The impact of Last Glacial climate variability in west-European loess revealed by radiocarbon dating of fossil earthworm granules. P. Natl. Acad. Sci. USA 114, 6209-6214, doi: 10.1073/pnas.1614751114, 2017.

Müller, U.C., Pross, J., and Bibus, E.: Vegetation response to rapid climate change in Central Europe during the past 140,000 yr based on evidence from the Füramoos pollen record. Quaternary Res. 59, 235-245, doi: 10.1016/S0033-5894(03)0005-X, 2003.

Nagashima, K., Tada, R., Tani, A., Sun, Y., Isozaki, Y., Toyoda, S., Hasegawa, H.: Millennial-scale oscillations of the westerly jet path during the last glacial period. J. Asian Earth Sci. 40, 1214-1220, 2011.

North Greenland Ice Core Project, members: High-resolution record of Northern Hemisphere climate extending into the last interglacial period. Nature 431, 147-151, doi: 10.1038/nature02805, 2004.

Rahmstorf, S.: Timing of abrupt climate change: A precise clock. Geophys. Res. Lett. 30, 17, doi:101029/102003GL017115, doi: 10.1029/2003GL017115, 2003.

Rasmussen, S.O., Bigler, M., Blockley, S.P., Blunier, T., Buchardt, S.L., Clausen, H.B., Cvijanovic, I., Dahl-Jensen, D., Johnsen, S.J., Fischer, H., Gkinis, V., Guillevic, M., Hoek, W.Z., Lowe, J.J., Pedro, J.B., Popp, T., Seierstad, I.K., Steffensen, J.P., Svensson, A.M., Vallelonga, P., Vinther, B.M., Walker, M.J.C., Wheatley, J.J., and Winstrup, M.: A stratigraphic framework for abrupt climatic changes during the Last Glacial period based on three synchronized Greenland ice-core records: refining and extending the INTIMATE event stratigraphy. Quaternary Sci. Rev. 106, 14-28, doi: 10.1016/j.quascirev.2014.09.007, 2014.

Rittner, M., Vermeesch, P., Carter, A., Bird, A., Stevens, T., Garzanti, E., Ando, S., Vezzoli, G., Dutt, R., Xu, Z.W., and Lu, H.Y.: The provenance of Taklamakan desert sand. Earth Planet. Sc. Lett. 437, 127-137, doi: 10.1016/j.epsl.2015.12.036, 2016.

Rousseau, D.-D., Boers, N., Sima, A., Svensson, A., Bigler, M., Lagroix, F., Taylor, S., and Antoine, P.: (MIS3 & 2) millennial oscillations in Greenland dust and Eurasian aeolian records: a paleosol perspective. Quaternary Sci. Rev. 169, çç-113, doi: 10.1016/j.quascirev.2017.05.020, 2017.

Rousseau, D.-D., Chauvel, C., Sima, A., Hatté, C., Lagroix, F., Antoine, P., Balkanski, Y., Fuchs, M., Mellett, C., Kageyama, M., Ramstein, G., and Lang, A.: European glacial dust deposits: Geochemical constraints on atmospheric dust cycle modeling. Geophys. Res. Lett. 41, 7666-7674, doi: 10.1002/2014GL061382, 2014.

Rousseau, D.D., Antoine, P., Gerasimenko, N., Sima, A., Fuchs, M., Hatté, C., Moine, O., Zoeller, L.: North Atlantic abrupt climatic events of the last glacial period recorded in Ukrainian loess deposits. Clim. Past 7, 221-234, doi: 10.5194/cp-7-221-2011, 2011.

Rousseau, D.D., Antoine, P., Hatté, C., Lang, A., Zöller, L., Fontugne, M., Ben Othman, D., Luck, J.M., Moine, O., Labonne, M., Bentaleb, I., Jolly, D.: Abrupt millennial climatic changes from Nussloch (Germany) Upper Weichselian eolian records during the Last Glaciation. Quaternary Sci. Rev. 21, 1577-1582, 2002.

Rousseau, D.D., Derbyshire, E., Antoine, P., and Hatté, C.: European loess records, in: Elias, S. (Ed.), Encyclopedia of Quaternary Science. Elsevier, Amsterdam, pp. 1440-1456, 2007a.

Rousseau, D.D., Sima, A., Antoine, P., Hatté, C., Lang, A., Zöller, L.: Link between European and North Atlantic abrupt climate changes over the last glaciation. Geophys. Res. Lett. 34, 22, L22713 doi: 10.1029/2007GL031716, 2007b.

Ruth, U., Wagenbach, D., Steffensen, J.P., Bigler, M.: Continuous record of microparticle concentration and size distribution in the central Greenland NGRIP ice core during the last glacial period. J. Geophys. Res.-Atmospheres 108, D3,4098, doi: 10.1029/2002JD002376, 2003.

Schulz, M.: On the 1470-year pacing of Dansgaard-Oeschger warm events. Paleoceanography 17, 2, 4.1-4.10, doi: 10.1029/2000PA000571, 2002.

Sima, A., Kageyama, M., Rousseau, D.D., Ramstein, G., Balkanski, Y., Antoine, P., and Hatté, C.: Modeling dust emission response to North Atlantic millennial-scale climate variations from the perspective of East European MIS3 loess deposits. Clim. Past 9, 1385-1402, doi: 10.5194/cp-9-1385-2013, 2013.

Sima, A., Rousseau, D.D., Kageyama, M., Ramstein, G., Schulz, M., Balkanski, Y., Antoine, P., Dulac, F., and Hatté, C.: Imprint of North-Atlantic abrupt climate changes on western European loess deposits as viewed in a dust emission model. Quaternary Sci. Rev. 28, 2851-2866, doi:10.1016/j.quascirev.2009.07.016, 2009.

Sodemann, H., Masson-Delmotte, V., Schwierz, C., Vinther, B.M., and Wernli, H.: Interannual variability of Greenland winter precipitation sources: 2. Effects of North Atlantic Oscillation variability on stable isotopes in precipitation. J. Geophys. Res.-Atmospheres 113, D112, doi: 10.1029/2007JD009416, 2008.

Sodemann, H., and Zubler, E.: Seasonal and inter-annual variability of the moisture sources for Alpine precipitation during 1995-2002. Int. J. Climatol. 30, 947-961, doi: 10.1002/joc.1932, 2010.

Solomon, S., Qin, D., Manning, M., Chen, Z.Y., Marquis, M., Averyt, K.B., Tignor, M., Miller, H.L., (eds.): Contribution of Working Group I to the Fourth Assessment Report of the Intergovernemental Panel on Climate Change. Cambridge University Press, Cambridge, 2007.

Steffensen, J.P., Andersen, K.K., Bigler, M., Clausen, H.B., Dahl-Jensen, D., Fischer, H., Goto-Azuma, K., Hansson, M., Johnsen, S.J., Jouzel, J., Masson-Delmotte, V., Popp, T., Rasmussen, S.O., Rothlisberger, R., Ruth, U., Stauffer, B., Siggaard-Andersen, M.L., Sveinbjornsdottir, A.E., Svensson, A., and White, J.W.C.: High-resolution Greenland Ice Core data show abrupt climate change happens in few years. Science 321, 680-684, doi: 0.1126/science.1157707, 2008.

Sun, Y., Clemens, S.C., Morrill, C., Lin, X., Wang, X., and An, Z.: Influence of Atlantic meridional overturning circulation on the East Asian winter monsoon. Nat. Geosci. 5, 46-49, doi: 10.1038/NGEO1326, 2012.

Svensson, A., Biscaye, P.E., and Grousset, F.E.: Characterization of late glacial continental dust in the Greenland Ice Core Project ice core. J. Geophys. Res.-Atmospheres 105, 4637-4656, doi: 10.1029/1999JD901093, 2000.

Thomas, A.M., Rupper, S., and Christensen, F.: Characterizing the statistical properties and interhemispheric distribution of Dansgaard-Oeschger events. J. Geophys. Res. 116, doi:10.1029/2010JD014834, 2011.

Wang, Y.J., Cheng, H., Edwards, R.L., Kong, X., Shao, X., Chen, S., Wu, J., Jiang, X., Wang, X., and An, Z.: Millenial- and orbital-scale changes in the East Asian monsoon over the past 224,000 years. Nature 451, 1090-1093, doi: 10.1038/nature06692, 2008.

Wang, Y.J., Cheng, H., Edwards, R.L., An, Z.S., Wu, J.Y., Shen, C.C., and Dorale, J.A.: A high-resolution absolute-dated late Pleistocene monsoon record from Hulu Cave, China. Science 294, 2345-2348, doi: 10.1126/science.1064618, 2001.

Wolff, E.W., Chappellaz, J., Blunier, T., Rasmussen, S.O., and Svensson, A.: Millennial-scale variability during the last glacial: The ice core record. Quaternary Sci. Rev. 29, 2828-2838, doi: 10.1016/j.quascirev.2009.10.013, 2010.

Yin, Q.Z., Berger, A., Driesschaert, E., Goosse, H., Loutre, M.F., and Crucifix, M.: The Eurasian ice sheet reinforces the East Asian summer monsoon during the interglacials 500,000 years ago. Clim. Past 4, 79-90, doi: 10.5194/cp-4-79-2008, 2008.

Zdanowicz, C., Hall, G., Vaive, J., Amelin, Y., Percival, J., Girard, I., Biscaye, P., and Bory, A.: Asian dustfall in the St. Elias Mountains, Yukon, Canada. Geochim. Cosmochim. Ac. 70, 3493-3507, doi: 10.1016/j.gca.2006.05.005, 2006.

Figure captions

Figure 1. Studied records in this paper. A Location of the different records over Greenland and Eurasia. B. Map of the European loess. Indication of the depth of the LGM maximum sea-level low stand, of the expansion of the Greenland, Iceland, British and Fennoscandinavian ice-sheets. Location of European key loess sequences. Map drawn by P. Antoine in Rousseau et al. (2014) modified

Figure 2. Stratigraphic correlations between Nussloch paleosols and NGRIP interstadials (GI) (modified from Rousseau et al., 2017). Map as in Fig. 1. $\delta^{18}O$ (‰, in blue) and the dust concentration (part/µl, in brown) records in the NGRIP ice core over the interval between 60 ka and 15 ka b2k. Nussloch stratigraphic column from Antoine et al. 2016 modified.

Figure 3. Nussloch stratigraphy with the identification of the loess and paleosol units as discussed in the text. Arrows indicate the time's arrow during the dust depositions (in blue) and paleosol developments (in red). Sedimentation and Mass accumulation (MAR) rates as estimated from NGRIP $\delta^{18}O$ and dust chronologies. The insert at the bottom of the figure explains how time should be read when considering European loess sequences. Nussloch stratigraphic column from Antoine et al. 2016 modified.

Figure 4. Map of the maximum extension of the last climate cycle ice-sheets in Northern Europe. Schematic location of the polar jet stream with location of regions or areas (in black) and of sites (in red) discussed in the text. $\delta^{18}O$ (‰, in blue) and the dust concentration (part/µl, in brown) records in the NGRIP ice core over the interval between 60 ka and 15 ka b2k. Dust concentrations are shown on a logarithmic scale. Map was compiled by Jürgen Ehlers available at http://www.qpg.geog.cam.ac.uk/lgmextent.html

Figure 5. Impact of Atlantic climate conditions over Eurasia. Modern monthly average wind speed, in ms^{-1}, at 850 hPa (A) and at 300 hPa (B) pressure levels for March, June, September, December and April (main dust emission month) over Eurasia. Wind vectors plotted over shading and contours at 3 $m\ s^{-1}$ interval. Data source: NCEP reanalysis monthly wind components on a 2.5 × 2.5° long/lat grid for the interval 1971–2000.

Table 1. NGRIP ice-core record. Estimates of NGRIP GI start, end and duration, GI abrupt transition start, end and duration (from Rousseau et al. submitted), Temperature reconstruction for the GI transitions as published by Kindler et al. (2014). a) and b) NGRIP transition dates determined visually and algorithmically, respectively.

Table 2. Nussloch loess sequence loess and paleosol units and their chronological equivalents (GS and GI) in the NGRIP ice-core record. a) and b) NGRIP transition dates determined visually and algorithmically respectively.

Tab. 1A

Algorithm

GI	GI algorithmcally			Transition			Transition by Kindler	GI
	a)	b)	c)	d)	e)	f)		
#	δ180startAlgorithm-rounded (yr b2k)	δ180endtAlgorithm-rounded (yr b2k)	δ18durationAlgorithm-rounded (yr)	δ180start Transition Algorithm-(yr b2k)	δ180end Transition Algorithm-(yr b2k)	GIδ18OdurationAlgorithm (yr)	Tp difference(° C) Fig. 3	#
2	23380	23110	270	23375	23345	30	-8,5	2
3	27790	27460	330	27790	27765	25	-14,5	3
4	28910	28510	400	28910	28875	35	-12,5	4
5	32520	32030	500	32520	32490	30	-12,5	5
6	33740	33390	350	33735	33700	35	-9,5	6
7	35510	34730	780	35505	35440	65	-15,5	7
8	38240	36590	1650	38235	38200	35	-10	8
9	40170	39940	230	40165	40155	10	-6,5	9
10	41480	40790	690	41480	41440	40	-13,5	10
11	43370	42100	1270	43365	43315	50	-16,5	11
12	46860	44290	2580	46860	46830	30	-12,5	12
13	49320	49110	210	49315	49260	55	-8,5	13
14	54240	49410	4830	54235	54185	50	-12,5	14
15.1	55010	54750	260	55005	54975	30		15.1
15.2	55820	55300	520	55815	55765	50	-10	15.2
16.1	58050	56470	1590	58050	58020	30		16.1
16.2	58280	56440	1840	58280	58245	35	-10	16.2
17.1	59080	58520	570	59080	59060	20	-12,5	17.1
Mean			1048,33			36,39	-11,59	Mean
Std deviation			1163,44			13,37	2,74	Std deviation
Max			4830,00			65,00	-6,50	Max
Min			210,00			10,00	-16,50	Min
	aa)	bb)	cc)	dd)	ee)	ffl)		
#	duststartAlgorithm-rounded (yr b2k)	dustendtAlgorithm-rounded (yr b2k)	dustdurationAlgorithm-rounded (yr)	duststart Transition Algorithm-(yr b2k)	dustend Transition Algorithm-(yr b2k)	GIdustdurationAlgorithm (yr)	Tp difference(° C) Fig. 3	#
2	23430	22820	540	23430	23350	80	-8,5	2
3	27800	27520	250	27795	27770	25	-14,5	3
4	28940	28510	370	28935	28870	65	-12,5	4
5	32570	31780	680	32565	32450	115	-12,5	5
6	33750	33320	390	33750	33710	40	-9,5	6
7	35500	34620	830	35500	35445	55	-15,5	7
8	38260	36560	1640	38255	38195	60	-10	8
9	40190	39940	170	40185	40105	80	-6,5	9
10	41490	40800	640	41490	41440	50	-13,5	10
11	43370	42190	1120	43365	43310	55	-16,5	11
12	46910	44110	2720	46910	46825	85	-12,5	12
13	49310	48420	830	49305	49250	55	-8,5	13
14	54240	49480	4710	54240	54185	55	-12,5	14
15.1	55050	54770	220	55045	54985	60		15.1
15.2	55790	55390	370	55790	55755	35	-10	15.2
16.1	58050	56470	1550	58050	58015	35		16.1
16.2	58310	56360	1890	58310	58250	60	-10	16.2
17.1	59110	58530	510	59110	59040	70	-12,5	17.1
Mean			1079,44			60,00	-11,59	Mean
Std deviation			1134,87			21,21	2,74	Std deviation
Max			4710,00			115,00	-6,50	Max
Min			170,00			25,00	-16,50	Min

Tab 1B

Visual

GI	GI algorithmcally			Transition			Transition by Kindler	GI
	a)	b)	c)	d)	e)	f)		
#	δ180startVisual-rounded (yr b2k)	δ180endtVisual-rounded (yr b2k)	δ18duration Visual-rounded (yr)	δ180start Transition Visual (yr b2k)	δ180end Transition Visual- (yr b2k)	δ18O duration Visual (yr)	Tp difference(° C) Fig. 3	#
2	23370	23180	200	23373	23320	53	-8,5	2
3	27800	27470	330	27795	27758	37	-14,5	3
4	28910	28510	400	28907	28873	34	-12,5	4
5	32520	32030	500	32517	32458	59	-12,5	5
6	33750	33370	380	33748	33671	77	-9,5	6
7	35490	34640	850	35491	35431	60	-15,5	7
8	38230	36600	1640	38234	38189	45	-10	8
9	40180	39870	320	40184	40125	59	-6,5	9
10	41480	40780	700	41480	41424	56	-13,5	10
11	43360	42280	1090	43361	43312	49	-16,5	11
12	46890	44280	2610	46893	46802	91	-12,5	12
13	49300	48470	840	49300	49246	54	-8,5	13
14	54230	50030	4200	54229	54175	54	-12,5	14
15.1					0			15.1
15.2	55830	55400	430	55827	55747	80	-10	15.2
16.1					0			16.1
16.2	58280	56450	1830	58277	58235	42	-10	16.2
17.1	59080	58550	530	59078	59042	36	-12,5	17.1
Mean			1053,13			55,38	-11,59	Mean
Std deviation			1068,43			16,12	2,74	Std deviation
Max			4200,00			91,00	-6,50	Max
Min			200,00			34,00	-16,50	Min
	aa)	bb)	cc)	dd)	ee)	ffl)		
#	duststartVisual-rounded (yr b2k)	dustendtVisual-rounded (yr b2k)	dustdurationVisual-rounded (yr)	duststart Transition Visual (yr b2k)	dustend Transition Visual- (yr b2k)	dust duration Visual (yr)	Tp difference(° C) Fig. 3	#
2	23370	23190	180	23366	23308	58	-8,5	2
3	27800	27510	280	27795	27755	40	-14,5	3
4	28910	28530	390	28911	28881	30	-12,5	4
5	32500	31860	640	32504	32445	59	-12,5	5
6	33750	33310	430	33746	33677	69	-9,5	6
7	35490	34620	870	35485	35415	70	-15,5	7
8	38220	36540	1680	38221	38182	39	-10	8
9	40180	39900	290	40184	40075	109	-6,5	9
10	41490	40780	710	41487	41432	55	-13,5	10
11	43360	42200	1160	43361	43323	38	-16,5	11
12	46870	44190	2680	46866	46799	67	-12,5	12
13	49300	48420	880	49300	49243	57	-8,5	13
14	54210	50010	4200	54214	54160	54	-12,5	14
15.1								15.1
15.2	55810	55380	430	55811	55732	79	-10	15.2
16.1								16.1
16.2	58290	56380	1910	58292	58250	42	-10	16.2
17.1	59070	58540	530	59068	59026	42	-12,5	17.1
Mean			1078,75			56,75	-11,59	Mean
Std deviation			1078,95			19,61	2,74	Std deviation
Max			4200,00			109,00	-6,50	Max
Min			180,00			30,00	-16,50	Min

Tab.2A

Visual

Eolian sedimentation	Paleosols	Thickness depth (m)	Age end d18O (yr)	Age start d18O(yr)	Duration d18O (yr)	Sedimentation rate d18O (mm/yr)	Age end dust (yr)	Age start dust (yr)	Duration dust (yr)	Sedimentation rate dust (mm/yr)	MAR d18O (g/m2/yr)	MAR dust (g/m2/yr)	sed rate d18O cm/kyr	sed rate dust cm/kyr
Top sequece - Top G7 (GI2)		3,589	15000	23180	8180	0,44	15000	23190	8190	0,44	724	723	43,87	43,82
	G7 (GI2)	0,508	23180	23370	190		23190	23370	180					
Top G7 - Top G4 (GI3)		4,137	23370	27470	4100	1,01	23370	27510	4140	1,00	1665	1649	100,90	99,93
	G4 (GI3)	0,411	27470	27800	330		27510	27800	290					
Top G4 - Top G3 (GI4)		1,113	27800	28510	710	1,57	27800	28530	730	1,52	2586	2515	156,75	152,45
	G3 (GI4)	0,387	28510	28910	400		28530	28910	380					
Top G3 - Top G2b (GI5)		2,306	28910	32030	3120	0,74	28910	31860	2950	0,78	1220	1290	73,92	78,18
	G2b (GI5)	0,290	32030	32520	490		31860	32500	640					
Top G2b - Top G2a (GI6)		0,492	32520	33370	850	0,58	32500	33310	810	0,61	955	1002	57,87	60,73
	G2a (GI6)	0,444	33370	33750	380		33310	33750	440					
Top G2a - Top G1b (GI7)		0,831	33750	34640	890	0,93	33750	34620	870	0,95	1540	1575	93,33	95,48
	G1b (G7)	0,145	34640	35490	850		34620	35490	870					
Top G1b - Top LB (GI8)		0,363	35490	36600	1110	0,33	35490	36540	1050	0,35	539	570	32,69	34,56
	LB (GI8)	0,452	36600	38230	1630		36540	38220	1680					
Top LB - Top Gm3 (GI9)		0,831	38230	39870	1640	0,51	38220	39900	1680	0,49	836	816	50,65	49,44
	Gm3 (GI9)	0,347	39870	40180	310		39900	40180	280					
Top Gm3 - Top Gm2 (GI10)		0,710	40180	40780	600	1,18	40180	40780	600	1,18	1952	1952	118,28	118,28
	Gm2 (GI10)	0,298	40780	41480	700		40780	41490	710					
?			41480	42280	800		41490	42200	710					
	TK1 (GI11)		42280	43360	1080		42200	43360	1160					
unitX - Top GBU (GI12)		0,210	43360	44280	920	0,23	43360	44190	830	0,25	376	417	22,79	25,26
	GBU (GI12)	0,508	44280	46890	2610		44190	46870	2680					
Top GBU - Top Gm1 (GI13)		0,371	46890	48470	1580	0,23	46870	48420	1550	0,24	387	395	23,48	23,93
	Gm1 (GI13)	0,218	48470	49300	830		48420	49300	880					
Top Gm1 - Top GBL (GI14)		0,500	49300	50030	730	0,68	49300	50010	710	0,70	1130	1162	68,49	70,42
	GBL (GI14)	1,016	50030	54230	4200		50010	54210	4200					
mean					1508,85	0,70			1508,08	0,71	1159	1172	70,25	71,04
standard dev					1744,06	0,41			1744,54	0,40	674	654	40,86	39,66
Max					8180,00	1,57			8190,00	1,52	2586	2515	156,75	152,45
Min					190,00	0,23			180,00	0,24	376	395	22,79	23,93

Tab.2B

Agorithm

Eolian sedimentation	Paleosols	Thickness depth (m)	Age end d18O (yr)	Age start d18O(yr)	Duration d18O (yr)	Sedimentation rate (mm/yr)	Age end dust (yr)	Age start dust (yr)	Duration dust (yr)	Sedimentation rate (mm/yr)	MAR d18O (g/m2/yr)	MAR dust (g/m2/yr)	sed rate d18O cm/kyr	sed rate dust cm/kyr
Top sequece - Top G7 (GI2)		3,589	15000	23310	8310	0,43	15000	22820	7820	0,46	713	757	43,19	45,89
	G7 (GI2)	0,508	23310	23380	70		22820	23430	610					
Top G7 - Top G4 (GI3)		4,137	23380	27460	4080	1,01	23430	27520	4090	1,01	1673	1669	101,40	101,15
	G4 (GI3)	0,411	27460	27790	330		27520	27800	280					
Top G4 - Top G3 (GI4)		1,113	27790	28150	360	3,09	27800	28510	710	1,57	5101	2586	309,14	156,75
	G3 (GI4)	0,387	28150	28910	760		28510	28940	430					
Top G3 - Top G2b (GI5)		2,306	28910	32030	3120	0,74	28940	31780	2840	0,81	1220	1340	73,92	81,21
	G2b (GI5)	0,290	32030	32520	490		31780	32570	790					
Top G2b - Top G2a (GI6)		0,492	32520	33390	870	0,57	32570	33320	750	0,66	933	1082	56,54	65,59
	G2a (GI6)	0,444	33390	33740	350		33320	33750	430					
Top G2a - Top G1b (GI7)		0,831	33740	34730	990	0,84	33750	34620	870	0,95	1384	1575	83,90	95,48
	G1b (G7)	0,145	34730	35510	780		34620	35500	880					
Top G1b - Top LB (GI8)		0,363	35510	36590	1080	0,34	35500	36560	1060	0,34	554	565	33,60	34,24
	LB (GI8)	0,452	36590	38240	1650		36560	38260	1700					
Top LB - Top Gm3 (GI9)		0,831	38240	39940	1700	0,49	38260	39940	1680	0,49	806	816	48,86	49,44
	Gm3 (GI9)	0,347	39940	40170	230		39940	40190	250					
Top Gm3 - Top Gm2 (GI10)		0,710	40170	40790	620	1,14	40190	40800	610	1,16	1889	1920	114,46	116,34
	Gm2 (GI10)	0,298	40790	41480	690		40800	41490	690					
?			41480	42100	620		41490	42190	700					
	TK1 (GI11)		42100	43370	1270		42190	43370	1180					
unitX - Top GBU (GI12)		0,210	43370	44290	920	0,23	43370	44110	740	0,28	376	468	22,79	28,33
	GBU (GI12)	0,508	44290	46860	2570		44110	46910	2800					
Top GBU - Top Gm1 (GI13)		0,371	46860	49110	2250	0,16	46910	48420	1510	0,25	272	405	16,49	24,57
	Gm1 (GI13)	0,218	49110	49320	210		48420	49310	890					
Top Gm1 - Top GBL (GI14)		0,500	49320	49410	90	5,56	49310	49480	170	2,94	9167	4853	555,56	294,12
	GBL (GI14)	1,016	49410	54240	4830		49480	54240	4760					
Mean					1509,23	1,22			1509,23	0,91	2007	1503	121,65	91,09
Standard dev					1847,47	1,57			1726,75	0,75	2594	1243	157,21	75,32
Max					8310,00	5,56			7820,00	2,94	9167	4853	555,56	294,12
Min					70,00	0,16			170,00	0,25	272	405	16,49	24,57

Fig. 1

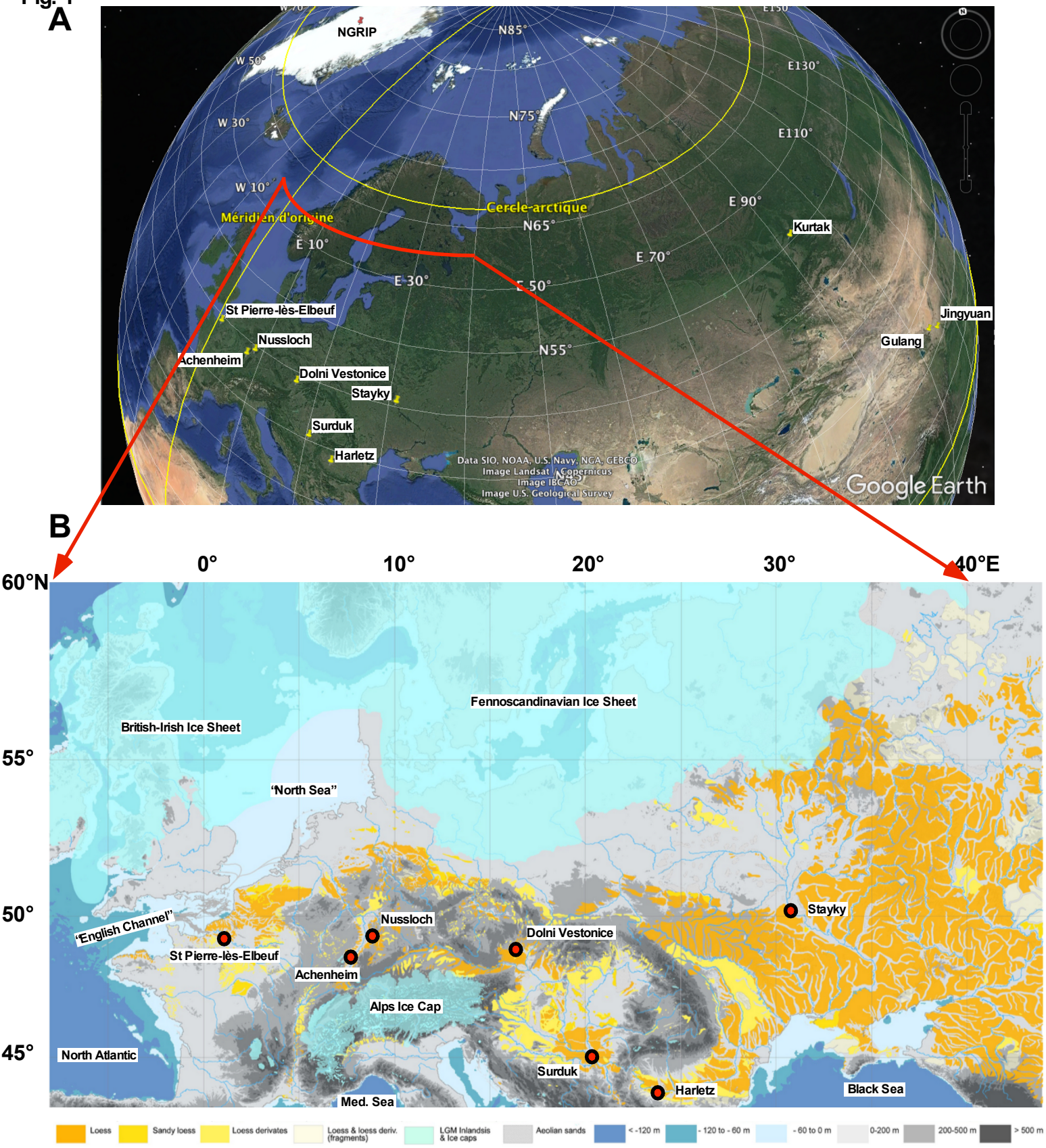
A
NGRIP
N85°
W 50°
E130°
W 30°
N75°
E110°
W 10°
Méridien d'origine
Cercle arctique
E 90°
N65°
Kurtak
E 10°
E 70°
E 30°
E 50°
St Pierre-lès-Elbeuf
Jingyuan
Nussloch
Gulang
N55°
Achenheim
Dolni Vestonice
Stayky
Surduk
Harletz
Data SIO, NOAA, U.S. Navy, NGA, GEBCO
Image Landsat / Copernicus
Image IBCAO
Image U.S. Geological Survey
Google Earth
B
0°
10°
20°
30°
40°E
60°N
55°
50°
45°
Fennoscandinavian Ice Sheet
British-Irish Ice Sheet
"North Sea"
"English Channel"
Nussloch
Stayky
Dolni Vestonice
St Pierre-lès-Elbeuf
Achenheim
Alps Ice Cap
North Atlantic
Surduk
Harletz
Black Sea
Med. Sea
Loess
Sandy loess
Loess derivates
Loess & loess deriv. (fragments)
LGM Inlandsis & Ice caps
Aeolian sands
< -120 m
- 120 to - 60 m
- 60 to 0 m
0-200 m
200-500 m
> 500 m

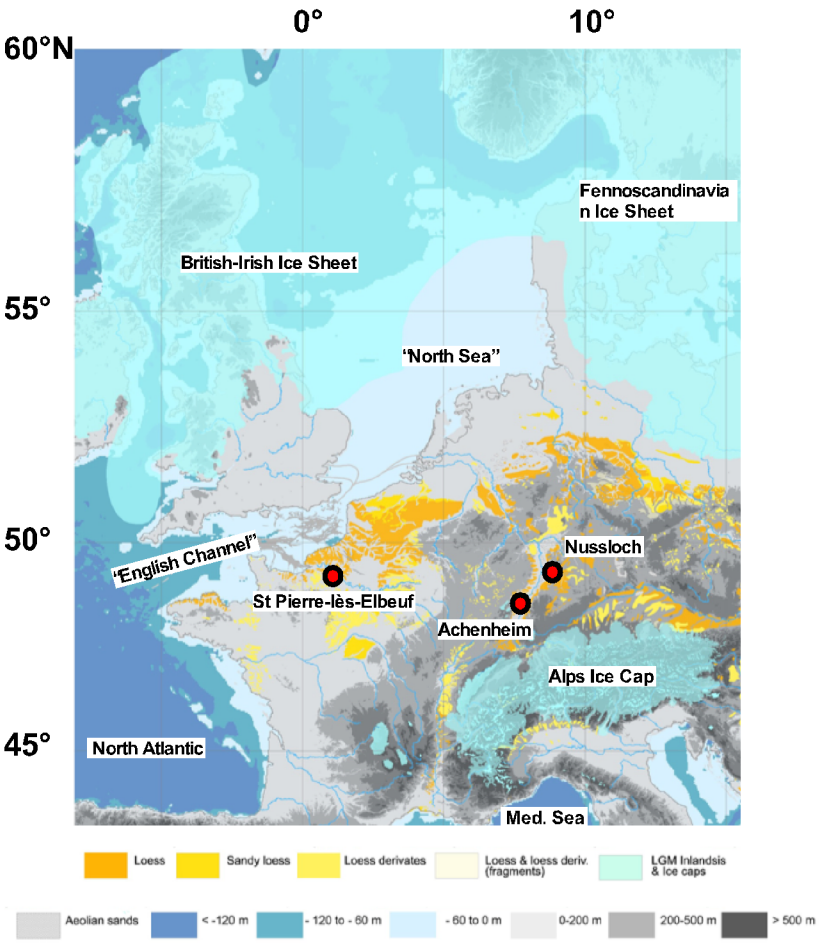
0°
10°
60°N
55°
50°
45°
Fennoscandinavian Ice Sheet
British-Irish Ice Sheet
"North Sea"
"English Channel"
Nussloch
St Pierre-lès-Elbeuf
Achenheim
Alps Ice Cap
North Atlantic
Med. Sea
Loess
Sandy loess
Loess derivates
Loess & loess deriv. (fragments)
LGM Inlandsis & Ice caps
Aeolian sands
< -120 m
- 120 to - 60 m
- 60 to 0 m
0-200 m
200-500 m
> 500 m

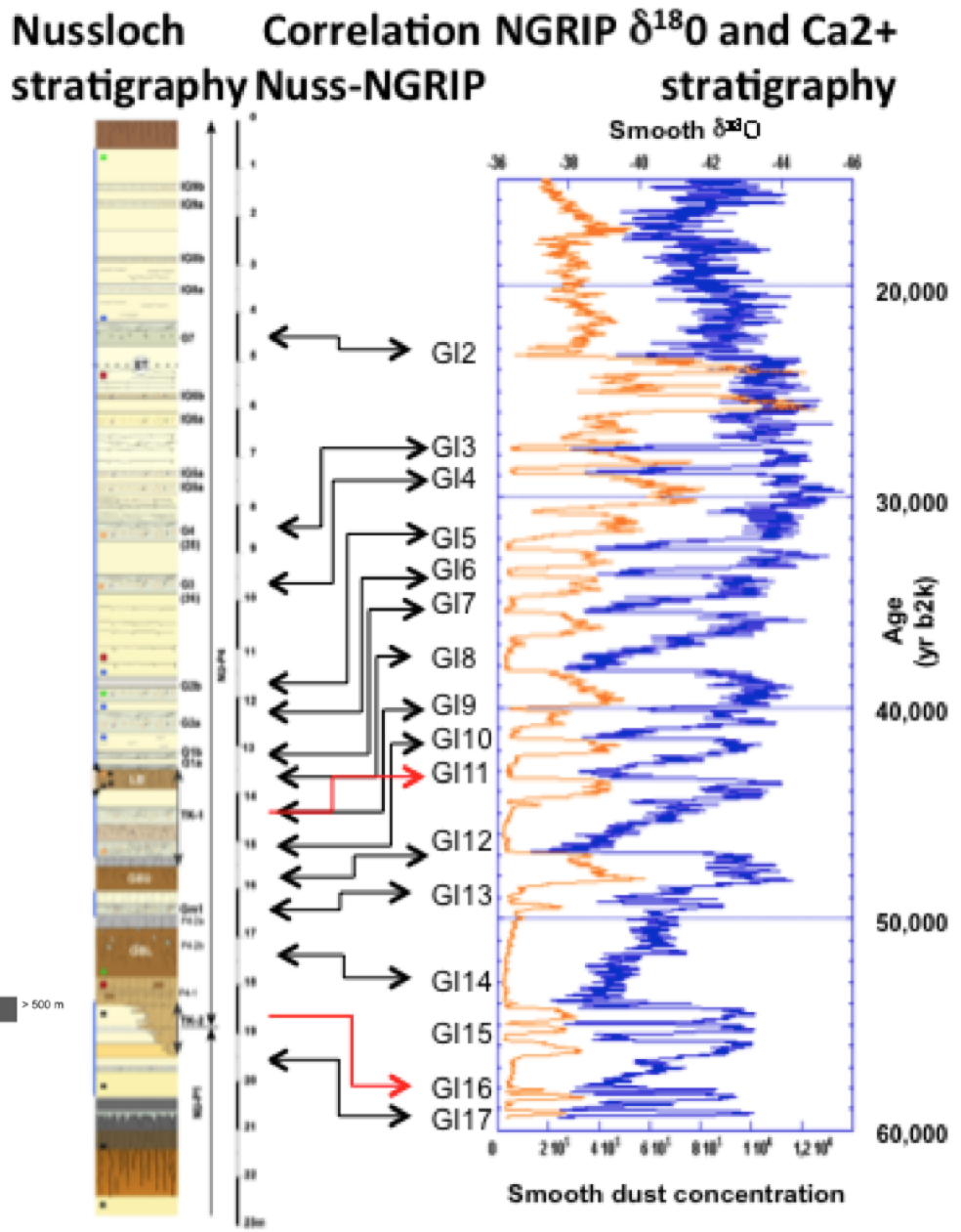
Nussloch stratigraphy
Correlation NGRIP δ18O and Ca2+ stratigraphy Nuss-NGRIP
Smooth δ18O
GI2
GI3
GI4
GI5
GI6
GI7
GI8
GI9
GI10
GI11
GI12
GI13
GI14
GI15
GI16
GI17
20,000
30,000
40,000
50,000
60,000
Age (yr b2k)
Smooth dust concentration

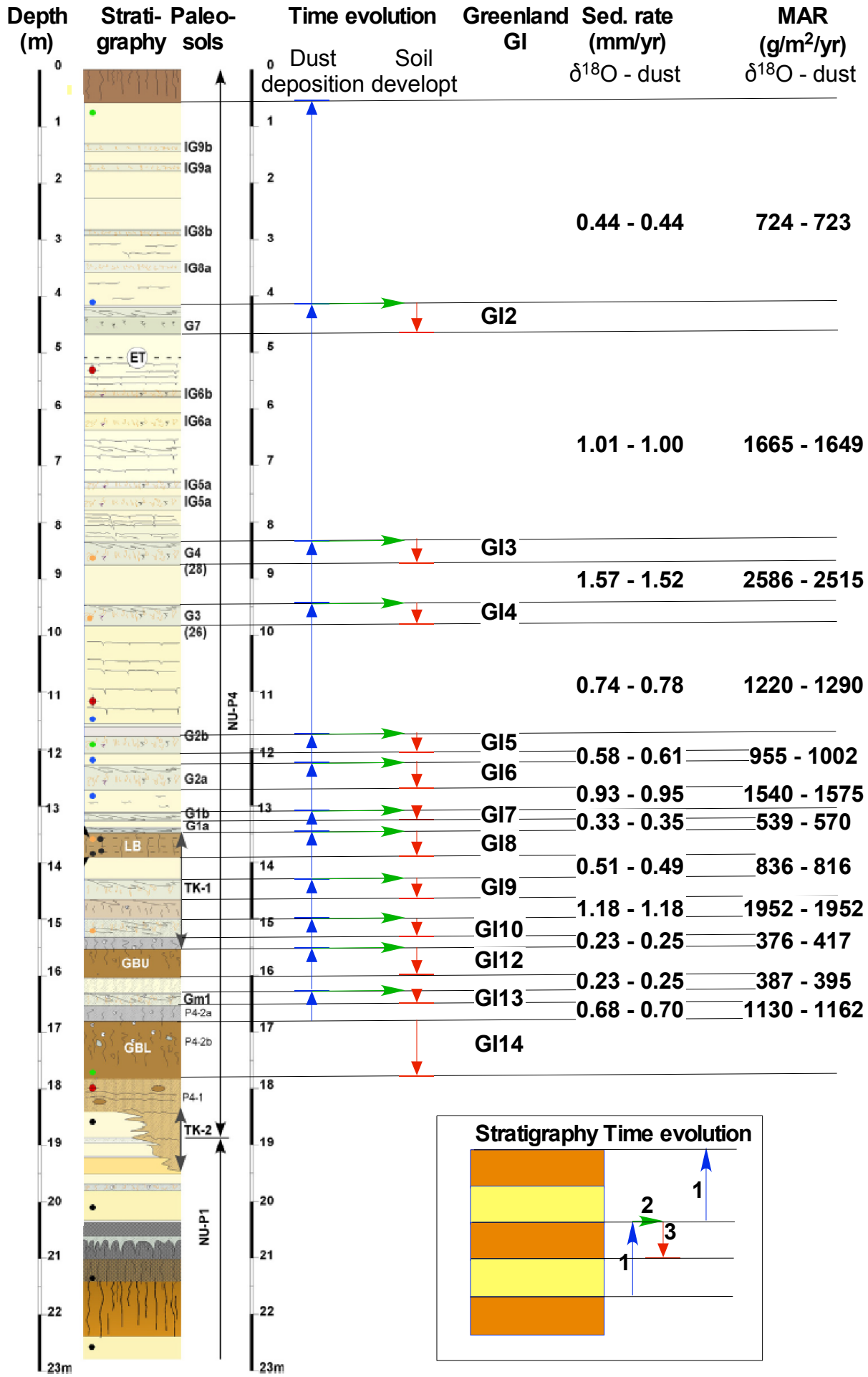
Depth (m)
Strati-graphy
Paleo-sols
Time evolution
Dust deposition
Soil developt
Greenland GI
Sed. rate (mm/yr)
δ18O - dust
MAR (g/m2/yr)
δ18O - dust
IG9b
IG9a
IG8b
IG8a
G7
ET
IG6b
IG6a
IG5a
IG5a
G4
(28)
G3
(26)
G2b
G2a
G1b
G1a
LB
TK-1
GBU
Gm1
P4-2a
GBL
P4-2b
P4-1
TK-2
NU-P4
NU-P1
GI2
GI3
GI4
GI5
GI6
GI7
GI8
GI9
GI10
GI12
GI13
GI14
0.44 - 0.44
724 - 723
1.01 - 1.00
1665 - 1649
1.57 - 1.52
2586 - 2515
0.74 - 0.78
1220 - 1290
0.58 - 0.61
955 - 1002
0.93 - 0.95
1540 - 1575
0.33 - 0.35
539 - 570
0.51 - 0.49
836 - 816
1.18 - 1.18
1952 - 1952
0.23 - 0.25
376 - 417
0.23 - 0.25
387 - 395
0.68 - 0.70
1130 - 1162
Stratigraphy Time evolution
1
2
3
1
23m
23m

Fig. 4

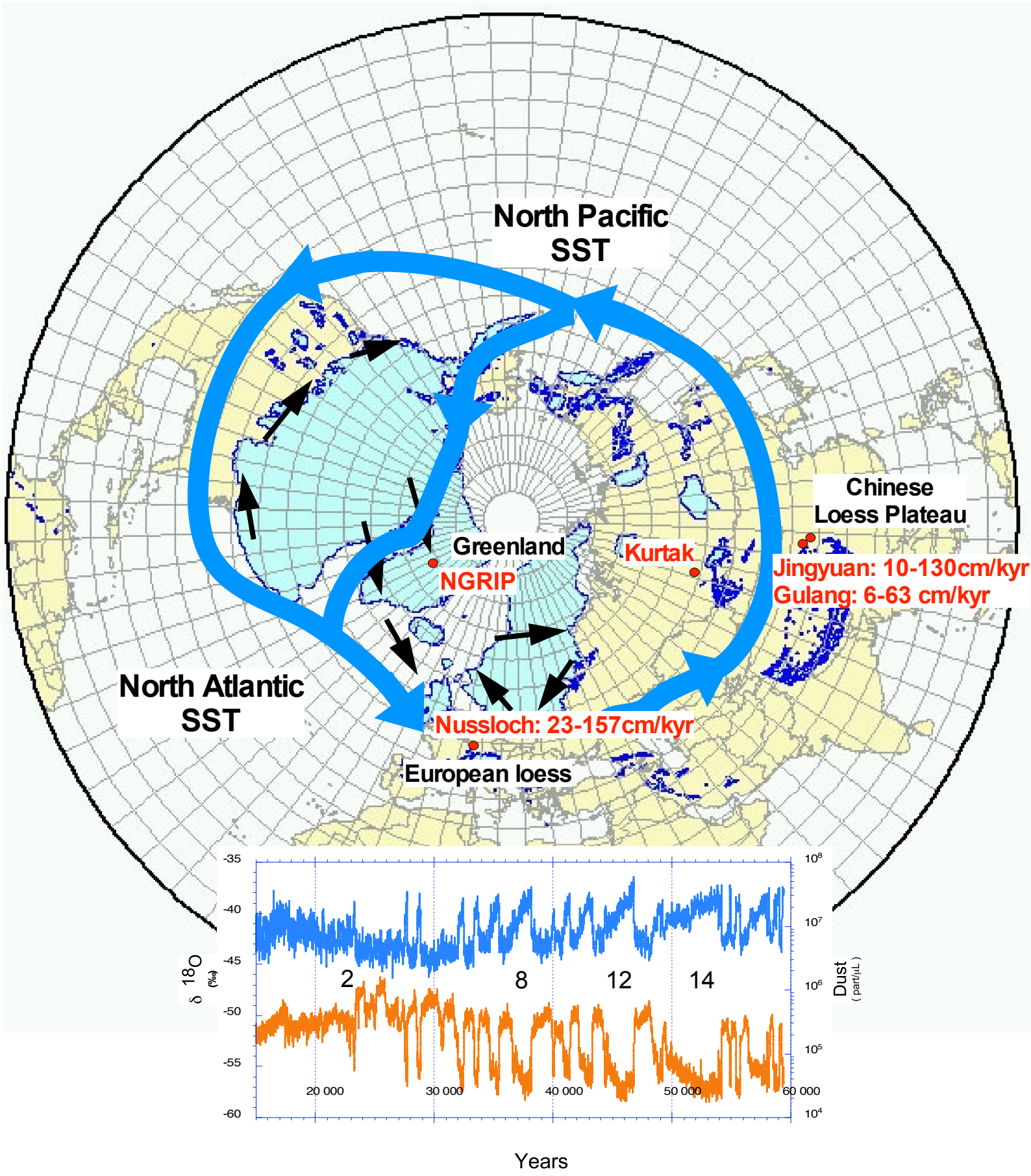
North Pacific
SST
Chinese
Loess Plateau
Greenland
NGRIP
Kurtak
Jingyuan: 10-130cm/kyr
Gulang: 6-63 cm/kyr
North Atlantic
SST
Nussloch: 23-157cm/kyr
European loess
δ 18O (‰)
Dust (part/µL)
2
8
12
14
20 000
30 000
40 000
50 000
60 000
Years

Fig. 5

A

1 Pressure 850.0 hPa Time Mar

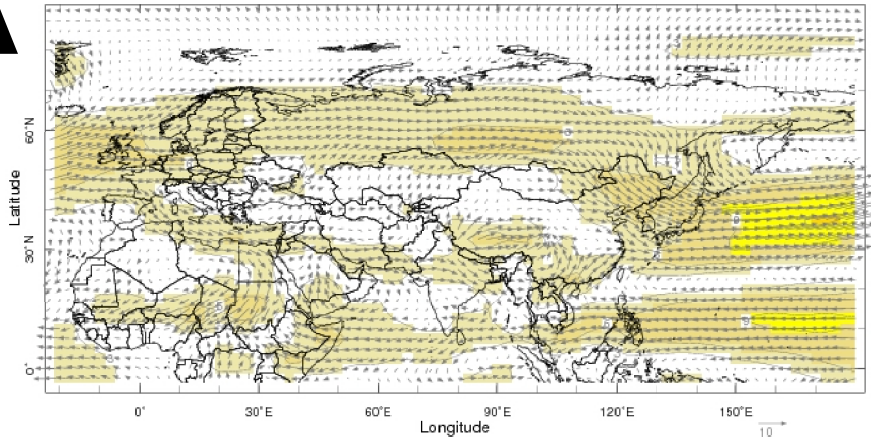

2 Pressure 850.0 hPa Time Jun

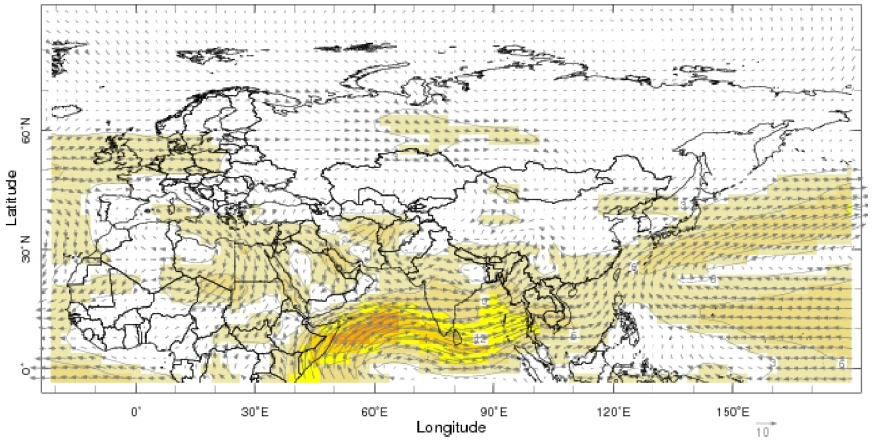

3 Pressure 850.0 hPa Time Sep

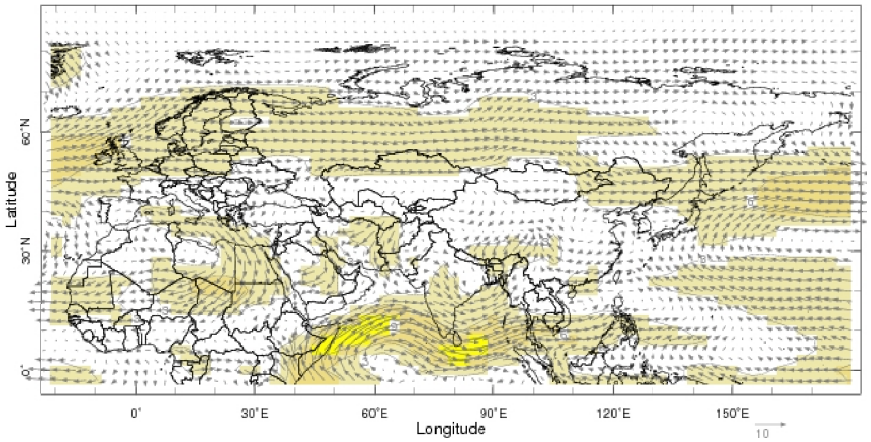

4 Pressure 850.0 hPa Time Dec

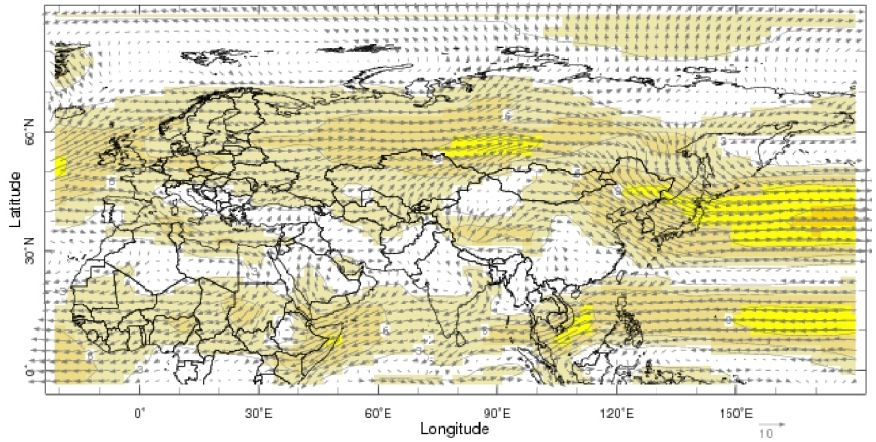

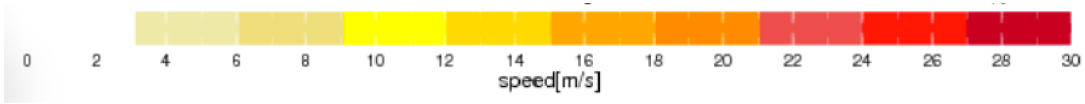

Fig. 5

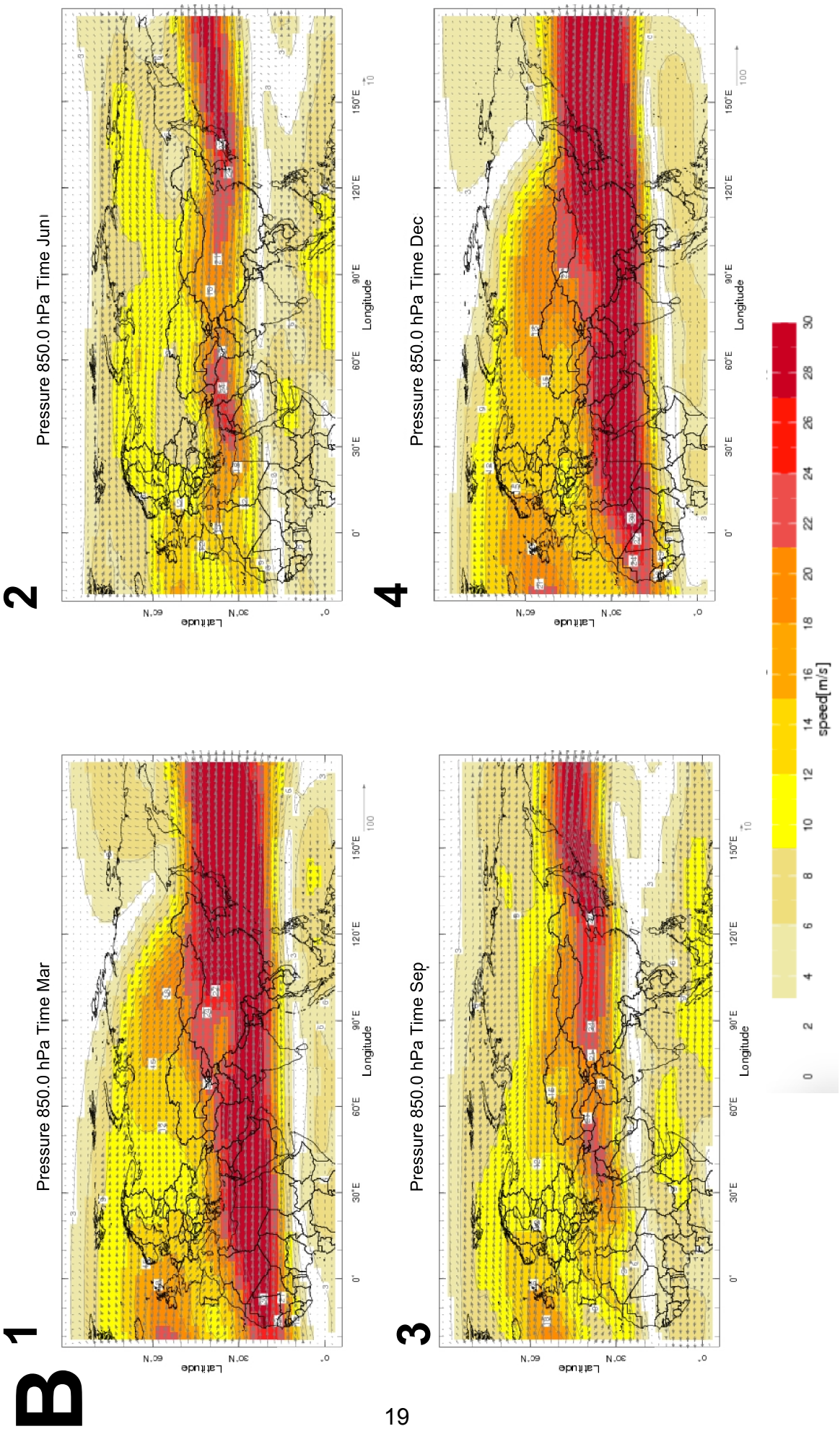
B
1
Pressure 850.0 hPa Time Mar
2
Pressure 850.0 hPa Time Jun
3
Pressure 850.0 hPa Time Sep
4
Pressure 850.0 hPa Time Dec
Latitude
Longitude
0°
30°N
60°N
0°
30°E
60°E
90°E
120°E
150°E
speed[m/s]
0
2
4
6
8
10
12
14
16
18
20
22
24
26
28
30